A sinus shear deformation model for static analysis of composite steel-concrete beams and twin-girder decks including shear lag and interfacial slip effects

M. Lezgy-Nazargah, Philippe Vidal, Olivier Polit

A sinus shear deformation model for static analysis of composite steel-concrete beams and twin-girder decks including shear lag and interfacial slip effects

M. Lezgy-Nazargah[a],[*], P. Vidal[b], O. Polit[b]

[a] *Faculty of Civil Engineering, Hakim Sabzevari University, Sabzevar, Iran*
[b] *LEME, UPL, Université Paris Nanterre, 50 rue de Sèvres, 92410 Ville d'Avray, France*

1. Introduction

Composite steel-concrete beams and decks are widely used in the construction of modern buildings, bridges and other civil engineering infrastructures. The optimal design of such structures requires accurate and realistic analysis tools. However, the accurate prediction of the structural behavior of composite beams and decks is a complicated procedure in some extent. In these types of structures, the concrete slab is usually connected to steel joists by steel shear connectors. Due to the flexibility of the shear connectors, the slips occur at the interface between the concrete slab and steel joists. This phenomenon which is also known as partial shear interaction [1] must be considered in the structural modeling for a realistic analysis. In the practical applications, twin-girder decks and steel-concrete beams are made of concrete slabs which are more than 20 m wide. In addition to partial shear interaction, the occurrence of significant warping in the concrete slab cross-section leads to axial stress concentration in the slab areas near the steel joists. This phenomenon which is known as shear lag effect cannot be neglected in the analysis of these structures. The above two aforementioned phenomena may be caught only with a 3D finite element (FE) analysis. However, the computational cost of the modeling of composite beams and decks with solid finite elements is very high and this type of

analysis must be carried out by expert designers.

These limitations encouraged researchers to develop advanced one-dimensional (1D) finite elements for the analysis of composite steel-concrete beams and decks. In the early developed 1D elements, the partial shear interaction effects were usually neglected but the shear lag effects was taken into account for design purposes using the concept of effective slab width [2]. Based on the Newmark's kinematic model, Sun [2] introduced a displacement based beam element for the accurate simulation of steel-concrete composite beams with shear lag and partial shear interaction. In this work, the effects of transverse shear strains in concrete slabs and steel beams are neglected. Sun and Bursi [3] formulated three displacement-based finite elements and two mixed (force-displacement based) elements for the static analysis of steel-concrete composite beams with partial shear interaction. They considered the effects of shear lag phenomenon by introducing a parabolic shear warping function in the kinematics of the slab cross-section. Based on Euler–Bernoulli's theory (EBT), a beam element with 13 dof was presented by Dezi et al. [5] for the analysis of steel-concrete twin-girder decks. By introducing a known warping function, Dezi et al. took into account the effects of slab shear lag. These researchers in [6] also extended their finite element formulation for the time-dependent analysis of twin girder steel-concrete composite decks. Luo et al. [7]

introduced a 1D finite segment beam model for the calculation of shear lag effects in the thin-walled box girders with varying depth. By solving the governing differential equations, they obtained multiple longitudinal displacement functions for each segment of the box girder. Based on the Generalised Beam Theory (GBT), Henriques et al. [8] introduced an accurate finite element model for nonlinear analysis of wide-flange steel and steel-concrete composite beams considering the shear lag effects. GBT can predict the in-plane and out-of-plane deformations of the cross-section by introducing "cross-section deformation modes".

By taking a third order variation of the axial displacement along the beam depth, Uddin et al. [9] proposed an efficient 1D beam finite element model for inelastic analysis of composite beams with partial shear interaction. Based on the third order shear deformation beam theory, Chakrabarti et al. [10] presented a finite element model for the analysis of steel-concrete composite beams. The model of these researchers takes into account the partial shear interaction effects as well as the transverse shear strains induced in the steel beam and concrete slab. In the framework of EBT and Timoshenko's beam theory (TBT), Zona and Ranzi [11] introduced three different 1D finite element models for the nonlinear analysis of steel-concrete composite members with beam-slab interface slip. A family of zero-thickness interface elements was introduced by Silva and Sousa [12] for the accurate analysis of steel-concrete composite beams with partial shear interaction. The proposed finite element formulation of these researchers is based on the assumption of the classical beam theories (EBT and TBT). Dall'Asta and Zona [13] investigated the locking problems which usually occur in the finite element analysis of composite beams with interlayer slip, or partial shear interaction. Through calibrated choice of the displacement shape functions, they proposed a strategy for avoiding locking in displacement-based elements. These researchers also compared the efficiency of the displacement-based and mixed finite elements models with each other. Ranzi et al. [14] analyzed the composite beams with partial shear interaction using different structural analysis approaches (the finite element method, the direct stiffness model, the finite difference method and the exact analytical method). They found that the exact analytical method and the direct stiffness approach lead to identical results. Based on the assumption of GBT, Taig et al. [15] introduced a 1D finite element model for investigation of the partial shear interaction phenomenon in steel–concrete composite beams.

For the realistic and accurate analysis of composite steel-concrete beams and decks, three kinematic aspects should be considered: effects of transverse shear strains in the concrete slab and steel joists, shear lag phenomenon and beam-slab interface slip. The review of open literature shows that the formulation available for the analysis of composite beams/decks involves only one or two of the above kinematic aspects. To fill this gap, a new advanced 1D kinematic and finite element model is developed in this study for static analysis of composite beams/decks. The proposed model takes into account the effects of shear lag and partial shear interaction. It also considers the effects of transverse shear strains induced in the concrete slab and steel beams which have an important role in the response of composite beams/decks particularly for those with deep depth. The present model is based on a Sinus deformation theory which satisfies the zero transverse shear stress conditions on the top and bottom surfaces of the composite beams/decks. For capturing the shear lag effects, the product of a known warping shape function at a unknown measuring intensity function is introduced in the slab cross-section kinematic. The slab-beam slip is modeled based on the concept of spring layer model. It is worth to note that the original Sinus model kinematics was first time introduced by Polit and Touratier [16] for the analysis of laminated composite plates. The Sinus shear deformation theory was enriched in Vidal and Polit [17] by introducing a layer refinement in the kinematics, and then extended to thermal (Vidal and Polit [18]) and piezoelectric (Lezgy-Nazargah et al. [19–21]) effects. In the present study, these last works are extended to static analysis of composite steel-concrete beams and twin-girder decks.
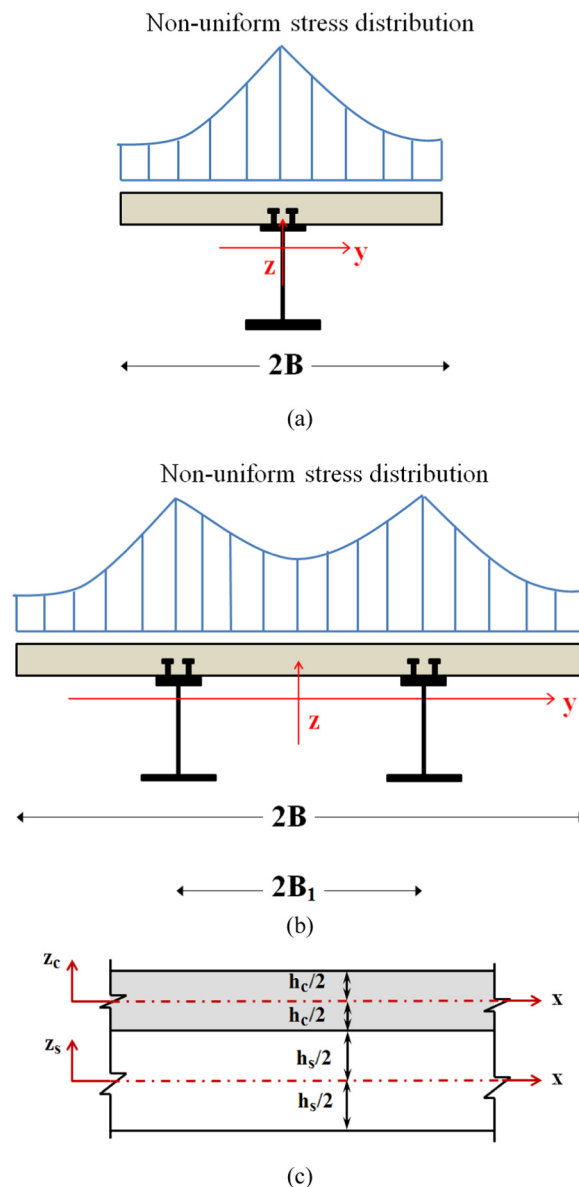

Fig. 1. Typical geometry of composite structures: (a) steel-concrete beam cross-section, (b) twin-girder deck cross-section, (c) side view of a portion of the composite structure.

Emphasis in this study is placed on the shear lag and interfacial slip effects, rather than on detailed nonlinear constitutive laws of concrete and steel.

Firstly, a three-nodded beam element with 25 dofs is developed based on the kinematics proposed for the concrete slab and steel joists. In the next step, steel-concrete composite beams and twin-girder decks with different loading and boundary conditions are analyzed using a MATLAB code whose algorithm is based on the present formulation. Finally, the results obtained from the present finite element model are compared with the elasticity solutions, the results of 3D FE analysis and other similar 1D FE models available in the open literature.

2. Problem formulation

The typical cross-section of steel-concrete composite beams and twin girder decks are depicted in Fig. 1. As shown in Fig. 1, these structures are made of the concrete slab, steel joists and shear connectors. The chosen Coordinate systems for each constituent element are also shown in these figures. Note that the coordinate systems are

chosen so that the coordinate plane *x-z* lies on the cross section symmetry plane of composite beam/deck.

2.1. Kinematics

In this study, the following relations are considered for the axial and vertical displacement components of the concrete slab:

$$U_c(x, y, z_c) = u_{0c}(x) - z_c \frac{\partial w(x)}{\partial x} + g(z_c)\left(\omega_c(x) + \frac{\partial w(x)}{\partial x}\right) + \psi(y)\, u_{lag}(x, z_c)$$

(1.a)

$$W_c(x, y, z) = w(x)$$

(1.b)

where u_{0c} is the axial displacement at the reference plane of the concrete slab, $\omega_c(x)$ denotes the shear-bending rotation of concrete slab around the y axis and $g(z_c) = (h_c/\pi)\sin(\pi z_c/h_c)$. w is the vertical (transverse) displacement which is taken to be same for both the concrete slab and steel beams. $\psi(y)$ is known warping shape function of concrete slab while $u_{lag}(x, z_c)$ is the corresponding warping intensity function. Expressions for $u_{lag}(x, z_c)$ and $\psi(y)$ are given in Section 2-2. In most of existing studies [3–5] that the effect of shear lag has been considered in the formulation, the intensity of warping shape function is assumed to be constant on the slab thickness (i.e. $u_{lag}(x, z_c) \cong u_{lag}(x)$). However, this simplifying assumption is valid only for steel-concrete composite beams with small thickness of the slab.

Concerning the steel beams, they are assumed as equivalent rec-

$$\tau_{xy} = \varphi_1(x)(y + B) + z_c \varphi_2(x)(y + B) + \sin\left(\frac{\pi z_c}{h_c}\right)\varphi_3(x)(y + B)$$

$$\tau_{xy} = \varphi_1(x)y + z_c \varphi_2(x)y + \sin\left(\frac{\pi z_c}{h_c}\right)\varphi_3(x)y$$

$$\tau_{xy} = \varphi_1(x)(y-B) + z_c \varphi_2(x)(y-B) + \sin\left(\frac{\pi z_c}{h_c}\right)\varphi_3(x)(y-B)$$

tangular layered composite structures [22–24] and the following relations are considered for their displacement fields:

$$U_s(x, y, z_s) = u_{0s}(x) - z_s \frac{\partial w(x)}{\partial x} + f(z_s)\left(\omega_s + \frac{\partial w(x)}{\partial x}\right)$$

(2.a)

$$W_s(x, y, z) = w(x)$$

(2.b)

where $f(z_s) = (h_s/\pi)\sin(\pi z_s/h_s)$, u_{0s} and $\omega_s(x)$ denote the axial displacement and the shear-bending rotation at the reference plane of steel joists, respectively.

2.2. Warping shape and intensity functions

For describing the non-uniform distribution of axial stress in the concrete slab, warping and intensity shape functions are introduced in this section.

The global equilibrium equations at any point of the concrete slab should also be satisfied:

$$\frac{\partial \sigma_{xx}}{\partial x} + \frac{\partial \tau_{xy}}{\partial y} + \frac{\partial \tau_{xz}}{\partial z} = 0$$

(3)

where σ_{xx}, τ_{xy} and τ_{xz} are components of Cauchy stress tensor. By assuming, at a first level of approximation, a uniform distribution of axial displacement on the slab width, the following expressions are obtained for stress components of concrete slab:

$$\sigma_{xx} = E_c \frac{du_{0c}(x)}{dx} - E_c \frac{d^2 w(x)}{\partial x^2} z_c + E_c \left(\frac{d\omega_c(x)}{dx} + \frac{d^2 w(x)}{\partial x^2}\right)\frac{h_c}{\pi}\sin\left(\frac{\pi z_c}{h_c}\right)$$

(4)

$$\tau_{xz} = G_c \left(\omega_c(x) + \frac{\partial w(x)}{\partial x}\right)\cos\left(\frac{\pi z_c}{h_c}\right)$$

(5)

where E_c and G_c denote modulus of elasticity and shear modulus of the concrete material, respectively. Note that Eqs. (4) and (5) are obtained based on the usual displacement-strain and stress-strain relations. It is seen from Eq. (5) that the transverse shear stress has a cosine variation over the slab thickness which becomes zero at the top surface of slab. It also becomes zero at the bottom surface of slab which is not true for the portion connected with the steel joists. However, this point should be considered here that the distributed shear springs, used for modeling the interfacial slip phenomenon, enforce the continuity conditions of transverse shear stress at the interface between the concrete slab and steel joists (see Section 2.3). Substituting the Eqs. (4) and (5) into Eq. (3) and renaming the unknown parameters gives:

$$\frac{\partial \tau_{xy}}{\partial y} + \varphi_1(x) + z_c \varphi_2(x) + \sin\left(\frac{\pi z_c}{h_c}\right)\varphi_3(x) = 0$$

(6)

Integrating of Eq. (6) by taking into account the boundary conditions of τ_{xy} give the following expressions for the in-plane shear stress at the concrete slab:

$$-B \leq y \leq -B_1$$

(7.a)

$$-B_1 < y < B_1$$

(7.b)

$$B_1 \leq y \leq B$$

(7.c)

Based on the usual displacement-strain and stress-strain relations, one can write:

$$\frac{\partial U_c(x, y, z)}{\partial y} = \frac{1}{G_c}\tau_{xy}$$

(8)

Integrating Eq. (8) with respect to y by taking into account Eq. (7) lead to the following expression for the axial displacement of the concrete slab:

$$U_c(x, y, z_c) = J(x, z_c) + \psi(y)\left(\frac{B^2}{2G}\varphi_1(x) + \frac{B^2}{2G}\varphi_2(x)z_c + \frac{B^2}{2G_c}\varphi_3(x)\sin\left(\frac{\pi z_c}{h_c}\right)\right)$$

(9)

where

$$\psi(y) = \begin{cases} \left(\frac{y}{B}\right)^2 + 2\frac{y}{B} + \frac{B_1}{B}\left(2 - \frac{B_1}{B}\right) & -B \leq y \leq -B_1 \\ \left(\frac{y}{B}\right)^2 - \left(\frac{B_1}{B}\right)^2 & -B_1 < y < B_1 \\ \left(\frac{y}{B}\right)^2 - 2\frac{y}{B} + \frac{B_1}{B}\left(2 - \frac{B_1}{B}\right) & B_1 \leq y \leq B \end{cases}$$

is warping functions and $J(x, z_c)$ is an unknown function. In the general case (twin-girder composite decks), the warping functions obtained for the slab cross-section are constituted by three parabolic branches. In the case in which $B_1 = 0$ (i.e. steel-concrete composite beams), the warping functions have only two parabolic branches. Distribution of the warping function $\psi(y)$ along the width of the concrete slab is shown in Fig. 2.

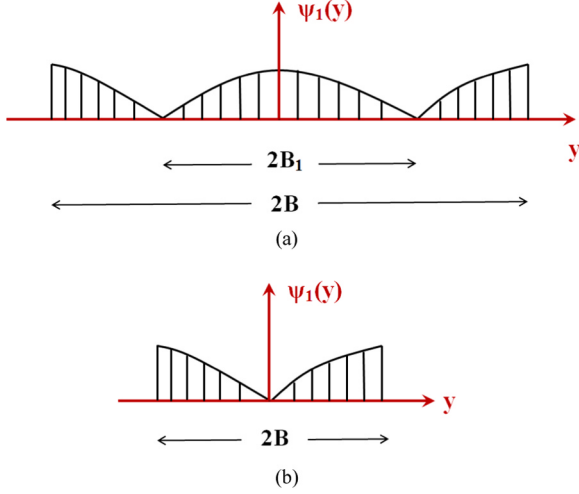By comparing the right side of Eq. (1.a) and Eq. (9), it can be

$$\mathbf{A_c} = \begin{bmatrix} 0 & \left(g\left(z\right)_c - z_c\right)\frac{d}{dx} & 0 & 1 & g\left(z\right)_c & \psi(y) & z_c\psi(y) & \sin\left(\frac{\pi z_c}{h_c}\right)\psi(y) \\ 0 & 1 & 0 & 0 & 0 & 0 & 0 & 0 \end{bmatrix}$$

The Green's strain vector in the concrete slab may be written as:

$$\varepsilon_\mathbf{c} = \mathbf{L_c u_u} \tag{14}$$

where $\varepsilon_\mathbf{c} = \{\varepsilon_{xx} \ \ \gamma_{xy} \ \ \gamma_{xz}\}^T$, and

$$\mathbf{L_c} = \begin{bmatrix} 0 & \left(g(z_c) - z_c\right)\frac{d^2}{dx^2} & 0 & \frac{d}{dx} & g(z_c)\frac{d}{dx} & \psi(y)\frac{d}{dx} & z_c\psi(y)\frac{d}{dx} & \sin\left(\frac{\pi z_c}{h_c}\right)\psi(y)\frac{d}{dx} \\ 0 & 0 & 0 & 0 & 0 & \frac{d\psi(y)}{dy} & z_c\frac{d\psi(y)}{dy} & \sin\left(\frac{\pi z_c}{h_c}\right)\frac{d\psi(y)}{dy} \\ 0 & \left(\frac{dg(z_c)}{dz} - \frac{dz_c}{dz} + 1\right)\frac{d}{dx} & 0 & 0 & \frac{dg(z_c)}{dz} & 0 & \frac{dz_c}{dz}\psi(y) & \frac{\pi}{h_c}\cos\left(\frac{\pi z_c}{h_c}\right)\psi(y) \end{bmatrix}$$

Similarly, Eq. (2) can be rewritten in the following matrix form:

$$\mathbf{u_s} = \mathbf{A_s u_u} \tag{15}$$

where $\mathbf{u_s} = \{U_s \ \ W_s\}^T$, and

$$\mathbf{A_s} = \begin{bmatrix} 1 & \left(f\left(z\right)_s - z_s\right)\frac{d}{dx} & f\left(z\right)_s & 0 & 0 & 0 & 0 & 0 \\ 0 & 1 & 0 & 0 & 0 & 0 & 0 & 0 \end{bmatrix}$$

Thus, the strain vector in the steel beams can be expressed as:

$$\varepsilon_\mathbf{s} = \mathbf{L_s u_u} \tag{16}$$

where $\varepsilon_\mathbf{s} = \{\varepsilon_{xx} \ \ \gamma_{xz}\}^T$, and

$$\mathbf{L_s} = \begin{bmatrix} \frac{d}{dx} & \left(f(z_s) - z_s\right)\frac{d^2}{dx^2} & f(z_s)\frac{d}{dx} & 0 & 0 & 0 & 0 & 0 \\ 0 & \left(\frac{df(z_s)}{dz} - \frac{dz_s}{dz} + 1\right)\frac{d}{dx} & \frac{df(z_s)}{dz} & 0 & 0 & 0 & 0 & 0 \end{bmatrix}$$

2.5. Constitutive equations

The stress-strain relation at any point of the concrete slab can be written as:

$$\begin{Bmatrix} \varepsilon_{xx} \\ \gamma_{xy} \\ \gamma_{xz} \end{Bmatrix} = \begin{bmatrix} 1/E_c & 0 & 0 \\ 0 & 1/G_c & 0 \\ 0 & 0 & 1/G_c \end{bmatrix} \begin{Bmatrix} \sigma_{xx} \\ \tau_{xy} \\ \tau_{xz} \end{Bmatrix} \tag{17}$$

or $\varepsilon_\mathbf{c} = \mathbf{D_c \sigma_c}$.

As hinted in Section 2.1, the steel joists are assumed as rectangular layered composite structures. In the framework of the equivalent layered section [22–24], the original cross-section of a thin-walled steel member is replaced with a unit width rectangular layered cross-section one. The stress-strain relations for the kth layer of the steel beam can be expressed as:

$$\begin{Bmatrix} \varepsilon_{xx}^{(k)} \\ \gamma_{xz}^{(k)} \end{Bmatrix} = \begin{bmatrix} 1/\bar{E}_s^{(k)} & 0 \\ 0 & 2(1+\nu_s)/\bar{E}_s^{(k)} \end{bmatrix} \begin{Bmatrix} \sigma_{xx}^{(k)} \\ \tau_{xz}^{(k)} \end{Bmatrix} \tag{18}$$

or $\varepsilon_s^{(k)} = \mathbf{D}_s^{(k)}\boldsymbol{\sigma}_s^{(k)}$. In the above equation, $\bar{E}_s^{(k)}$ denotes the modified modulus of elasticity of the kth layer of the equivalent cross-section of steel beam. ν_s is Poisson's ratio of the steel material. Due to this fact that the steel joist have small width, the in-plane component of the shear strain (γ_{xy}) is disregarded in Eq. (18). On the other hand, concrete slabs have in some practical applications more than 20 m wide. Thus, the effects of the in-plane shear strain γ_{xy} should be considered in the analysis (see Eq. (17)).

Fig. 2. Slab warping function: (a) twin-girder composite decks, (b) steel-concrete composite beams.

concluded

$$u_{lag}(x, z_c) = \frac{B^2}{2G}\varphi_1(x) + \frac{B^2}{2G}\varphi_2(x)z_c + \frac{B^2}{2G_c}\varphi_3(x)\sin\left(\frac{\pi z_c}{h_c}\right) \tag{10}$$

or

$$u_{lag}(x, z_c) = u_{1lag}(x) + u_{2lag}(x)z_c + u_{3lag}(x)\sin\left(\frac{\pi z_c}{h_c}\right) \tag{11}$$

Although the above expressions for $\psi(y)$ and $u_{lag}(x, z_c)$ were obtained by assuming a uniform distribution of axial displacement on the slab width, numerical experiences show that these expressions have enough accuracy for capturing shear lag phenomenon in the composite beams. For achieving more accurate expressions, the above process for derivation of $\psi(y)$ and $u_{lag}(x, z_c)$ should be repeated again with considering the last term of Eq. (1.a); i.e. $\psi(y) u_{lag}(x, z_c)$. The later process leads to the complicated algebraic expressions for $\psi(y)$ and $u_{lag}(x, z_c)$ without significant improvement of accuracy.

2.3. Slip model

The partial shear interaction effects are taken into account using distributed shear springs which connect the concrete slab and steel joists at their interface. The stiffness of these distributed elastic springs can be approximated based on the tangential stiffness of the shear connectors which connect two layers to each other. Thus, the slip which occurs at the interface between concrete slab and steel beams can be obtained from the following relation:

$$s = U_c(x, y = \pm B_1, z_c = -h_c/2) - U_s(x, y = \pm B_1, z_c = h_s/2) = \mathbf{A}_{spring}\mathbf{u_u} \tag{12}$$

where

$$\mathbf{A}_{spring} = [\mathbf{A}_{spring}^1 \ \ \mathbf{A}_{spring}^{21}]$$

$$\mathbf{A}_{spring}^1 = \left\{-1 \ \ (g(-h_c/2) - f(h_s/2) + (h_c + h_s)/2)\frac{d}{dx} \ \ -f(h_s/2) \ \ 1\right\}$$

$$\mathbf{A}_{spring}^2 = \{g(-h_c/2) \ \ \psi(y = \pm B_1) \ \ (-h_c/2)\psi(y = \pm B_1) \ \ -\psi(y = \pm B_1)\}$$

2.4. Expression of the strain

Eq. (1) can be written in the following matrix form:

$$\mathbf{u_c} = \mathbf{A_c u_u} \tag{13}$$

where $\mathbf{u_c} = \{U_c \ \ W_c\}^T$, $\mathbf{u_u} = \{u_s \ \ w \ \ \omega_s \ \ u_c \ \ \omega_c \ \ u_{1lag} \ \ u_{2lag} \ \ u_{3lag}\}^T$, and

3. Finite element formulation

3.1. Weak formulation of the boundary value problem

The total potential energy of the composite beam/deck can be written as:

$$\Pi = \frac{1}{2} \int_{V_s} \varepsilon_s^{\mathbf{T}} \sigma_s dV + \frac{1}{2} \int_{V_c} \varepsilon_c^{\mathbf{T}} \sigma_c dV + \frac{1}{2} \int_L k_w s^2 dx$$
$$- \int_L \mathbf{u}_s^T \bar{\mathbf{P}}_s \, dx - \int_{V_s} \mathbf{u}_s^T \bar{\mathbf{P}}_s^V \, dV - \int_L \mathbf{u}_c^T \bar{\mathbf{P}}_c \, dx - \int_{V_c} \mathbf{u}_c^T \bar{\mathbf{P}}_c^V \, dV \quad (19)$$

where $\bar{\mathbf{P}}_s$, $\bar{\mathbf{P}}_c$, $\bar{\mathbf{P}}_s^V$ and $\bar{\mathbf{P}}_c^V$ denote the steel surface force vector, concrete surface force vector, steel body force vector, and steel body force vector, respectively. V_s, V_c are steel joist volume and concrete slab volume, respectively. L is the total length of the composite beam/deck while k_w denotes the stiffness of the distributed shear springs.

3.2. Approximation of the boundary value problem

A 1D beam element is employed for solving the governing differential equations of the present formulation. To this aim, the unknown parameters $u_{os}(x)$, $w(x)$, $\omega_s(x)$, $u_{oc}(x)$, $\omega_c(x)$, $u_{1lag}(x)$, $u_{2lag}(x)$ and $u_{3lag}(x)$ are interpolated in terms of their nodal variables. C^1-continous Hermitian shape functions are employed for the interpolation of the transverse displacement $w(x)$. The quadratic Lagrange shape functions are used for the interpolation of $\omega_s(x)$ and $\omega_c(x)$. Although linear Lagrange shape functions are enough for the interpolation of rotation in slab and steel beams, the identical order of approximation in $dw(x)/dx$ and $\omega_i(x)(i = s, c)$ is prevented as the field compatibility conditions in the relevant transverse shear strain components of the concrete slab and steel beam are ensured [17–20]. $u_{os}(x)$, $u_{oc}(x)$, $u_{1lag}(x)$, $u_{2lag}(x)$ and $u_{3lag}(x)$ are also approximated by quadratic Lagrange shape functions. The employed three-node element as well as its nodal variables are shown in Fig. 3.

In the domain of each element, the vector of unknown parameters $\mathbf{u_u}$ can be expressed in terms of the nodal variables as follow:

$$\mathbf{u_u} = [\bar{\mathbf{N}} \quad \bar{\bar{\mathbf{N}}} \quad \underline{\mathbf{N}}] \begin{Bmatrix} \hat{\mathbf{u}}_1^e \\ \hat{\mathbf{u}}_3^e \\ \hat{\mathbf{u}}_2^e \end{Bmatrix} = \mathbf{N} \hat{\mathbf{u}}^e \quad (20)$$

where

$$\hat{\mathbf{u}}_1^e = \{(u_{os})_1 \ (w)_1 \ (\omega_s)_1 \ (w_{,x})_1 \ (u_{oc})_1 \ (\omega_c)_1 \ (u_{1lag})_1 \ (u_{2lag})_1 \ (u_{3lag})_1\}^T \hat{\mathbf{u}}_3^e$$
$$= \{(u_{os})_3 \ (\omega_s)_3 \ (u_{oc})_3 \ (\omega_c)_3 \ (u_{1lag})_3 \ (u_{2lag})_3 \ (u_{3lag})_3\}^T$$

$$\hat{\mathbf{u}}_2^e = \{(u_{os})_2 \ (w)_2 \ (\omega_s)_2 \ (w_{,x})_2 \ (u_{oc})_2 \ (\omega_c)_2 \ (u_{1lag})_2 \ (u_{2lag})_2 \ (u_{3lag})_2\}^T$$

and $\bar{\mathbf{N}}$, $\bar{\bar{\mathbf{N}}}$ and $\underline{\mathbf{N}}$ are the interpolation matrices. Substituting Eq. (20) into Eqs. (13) and (15) gives:

$$\mathbf{u_s} = \mathbf{A_s} \mathbf{N} \hat{\mathbf{u}}^e = \mathbf{N_s} \hat{\mathbf{u}}^e \quad (21)$$

$$\mathbf{u}_c = \mathbf{A_c} \mathbf{N} \hat{\mathbf{u}}^e = \mathbf{N_c} \hat{\mathbf{u}}^e \quad (22)$$

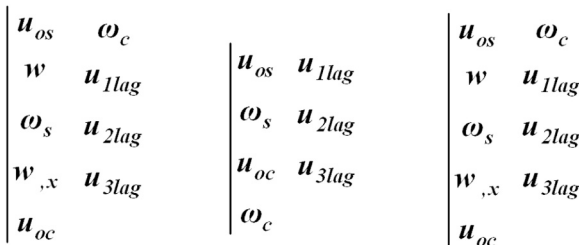Similarly, the steel and concrete strain vectors as well as the

Fig. 3. three-nodded beam element and its nodal variables.

expression obtained for slip may be written in terms of nodal variables:

$$\varepsilon_c = \mathbf{L}_c \mathbf{u_u} = \mathbf{L}_c \mathbf{N} \hat{\mathbf{u}}^e = \mathbf{B_c} \hat{\mathbf{u}}^e \quad (23)$$

$$\varepsilon_s = \mathbf{L}_s \mathbf{u_u} = \mathbf{L}_s \mathbf{N} \hat{\mathbf{u}}^e = \mathbf{B_s} \hat{\mathbf{u}}^e \quad (24)$$

$$s = \mathbf{A}_{spring} \mathbf{u_u} = \mathbf{A}_{spring} \mathbf{N} \hat{\mathbf{u}}^e = \mathbf{B}_{spring} \hat{\mathbf{u}}^e \quad (25)$$

Inserting Eqs. (21)–(25) into Eq. (19) gives the total potential energy of the composite beam/deck beam in terms of the nodal variables. Minimizing the total potential energy results:

$$\mathbf{K} \hat{\mathbf{u}} = \mathbf{P} \quad (26)$$

where is the total stiffness matrix, $\hat{\mathbf{u}}$ is the total unknown nodal vector, and P is the total load vector. The aforementioned matrices can be defined as follows:

$$\mathbf{K} = \sum_e \mathbf{K}_s^e + \sum_e \mathbf{K}_c^e + \sum_e \mathbf{K}_{spring}^e, \quad \mathbf{P} = \sum_e \mathbf{F}_s^e + \sum_e \mathbf{F}_c^e, \quad \hat{\mathbf{u}} = \sum_e \hat{\mathbf{u}}^e$$
$$(27)$$

The element steel joists stiffness matrix $\mathbf{K}_s^e$, the element concrete slab stiffness matrix $\mathbf{K}_c^e$, the element distributed shear spring stiffness matrix $\mathbf{K}_{spring}^e$, the element steel joists force vector $\mathbf{F}_s^e$, and the element concrete slab force vector $\mathbf{F}_c^e$ are defined, respectively, as below:

$$\mathbf{K}_s^e = \int_{V_s} \mathbf{B}_s^{\mathbf{T}} \mathbf{D}_s \mathbf{B}_s dV \quad (28)$$

$$\mathbf{K}_c^e = \int_{V_c} \mathbf{B}_c^{\mathbf{T}} \mathbf{D}_c \mathbf{B}_c dV \quad (29)$$

$$\mathbf{K}_{spring}^e = \int k_w \mathbf{B}_{spring}^{\mathbf{T}} \mathbf{B}_{spring} dx \quad (30)$$

$$\mathbf{F}_s^e = \int \mathbf{N}_s^T \bar{\mathbf{P}}_s \, dx + \int \mathbf{N}_s^T \bar{\mathbf{P}}_s^V \, dV \quad (31)$$

$$\mathbf{F}_c^e = \int \mathbf{N}_c^T \bar{\mathbf{P}}_c \, dx + \int \mathbf{N}_c^T \bar{\mathbf{P}}_c^V \, dV \quad (32)$$

In the region under hogging moment, the concrete slabs/decks are subjected to cracking. In order to consider the concrete crack of slabs/decks, the stiffness matrix of composite beam ($\mathbf{K}^e$) in the hogging regions should be calculated by neglecting the element stiffness matrix of concrete slab (i.e. $\mathbf{K}_c^e$).

4. Numerical results

In this section some numerical examples are presented to assess the efficiency of the proposed 1D finite element model for the static analysis of steel-concrete composite beams and twin-girder decks. The results obtained from the present finite element model are compared with the results of 3D finite element modeling (ABAQUS), exact elasticity solutions as well as the results of advanced 1D finite element models available in open literature.

4.1. Simply supported steel-concrete composite under uniformly distributed load

In this example, a simply supported steel-concrete composite beam with length L = 20 m under a uniformly distributed load of 35 kN/m is analyzed using the present finite element model. The geometrical parameters of the cross-section as well as the material properties of the concrete and steel are shown in Fig. 4.

First, a convergence study with respect to the number of elements was carried out. The maximum shear stress, maximum deflection and maximum slip of the composite beam for the non-dimensional interfacial spring stiffness parameter $\alpha L = 0.1$ are presented in Table 1. The definition of the non-dimensional interfacial stiffness αL is as below [13,14]:

$$\alpha L = L \sqrt{k_w \left(\frac{1}{E_c A_c} + \frac{1}{E_s A_s} + \frac{h_c^2 + h_s^2}{4(E_c I_c + E_s I_s)} \right)} \quad (33)$$
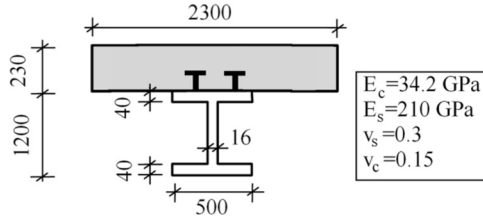
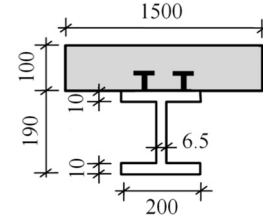**Fig. 4.** Geometry of the cross-section and the elastic characteristics of the materials (all dimensions in *mm*).

Fig. 5. The cross-section dimensions of the steel-concrete composite beam of example 2 (all dimensions in *mm*).

Table 1
Results of the mesh convergence study ($\alpha L = 0.1$).

Number of elements	Dof number	Maximum deflection (mm)	Maximum slip (mm)	Maximum shear stress (MPa)
5	89	21.10	2.3287	17.67
10	169	21.10	2.3286	18.62
20	329	21.10	2.3286	19.01
40	649	21.10	2.3286	19.12

where A_c and A_s denotes the cross-sectional area of the concrete slab and steel joist, respectively. I_c and I_s are the moment of inertia of the concrete slab and steel joist, respectively. It can be seen from Table 1 that the convergence velocity of the present finite element model is high and a mesh with 20 elements is enough for a static bending test.

It is worth to note that the considered beam of the present example has been previously studied by Chakrabarti et al. [10] using a family of finite element models which are based on TBT and high-order beam theory (HBT). In Table 2, the results of the present finite element model for different values of the non-dimensional interfacial stiffness αL are compared with those obtained by Chakrabarti et al. [10]. The results of all these different FE models are obtained using 20 beam elements of the same length. The number of dof of the present model, TBT and HBT are 329, 205 and 328, respectively. It can be seen from the Table 1 that the results of the present finite element model are in good agreement with the HBT of Chakrabarti et al. [10]. The computational cost of the present model is almost similar to HBT. However, the present finite element model, in contrast to HBT of Chakrabarti et al. [10], is able to take into accounts the effects of shear lag. The numerical results of Table 2 reveal this fact that with increasing of the non-dimensional interfacial stiffness αL, the values of the maximum deflection and induced transverse shear stress of the composite beam reduces significantly.

4.2. Simply supported steel-concrete composite beam under sinusoidal load

A simply supported steel-concrete composite beam subjected to a sinusoidal load with the amplitude of 15 kN/m is analyzed using the proposed finite element. The cross-section dimensions are depicted in Fig. 5. The considered beam has length L = 6 m and the shear stiffness of its shear connectors is assumed to be k_w. The considered values for

the modulus of elasticity and Poisson's ratio are $E_c = 8.5$ GPa and $v_c = 0.2$ for concrete, and $E_s = 210$ GPa and $v_s = 0.3$ for steel. Based on the convergence mesh study, it found that a mesh with 20 elements gives converged results for both displacements and stresses. Variations of the transverse shear stress of the composite beam along the thickness direction are shown in Fig. 6 for three different values of the shear stiffness of shear connectors (k_w = 40, 400, 4000 MPa). In this figure, the present finite element results are compared with the 2D exact elasticity solution of Xu and Wu [25]. It is seen that the present numerical results are in excellent agreement with elasticity solutions. It can be also observed from Fig. 6 that the present formulation ensures the zero boundary conditions of the transverse shear stress on the upper and lower surfaces of the composite beam. Fig. 6 also shows that with an increasing of the stiffness of the shear connectors, the transverse shear stress of the composite beam increases at the partially connected interface while it decreases at the web of steel joist.

Variations of the maximum deflection of the composite beam against different stiffness of shear connectors are depicted in Fig. 7. It is seen that the value of k_w has a significant effect on the flexural stiffness of the steel-concrete composite beams and it should be considered in practical design purposes.

4.3. Simply supported twin-girder composite deck

In this section, a simply supported twin-girder composite deck with span length L = 8 m is analyzed using the present finite element model. Uniformly distributed loads of 1 kN/m acting in the plane of steel webs are applied vertically to the considered composite deck. Cross-section dimensions and material properties of the beam are shown in Fig. 8. Distributions of the mid-span axial stress σ_{xx} at the concrete slab mid-height are shown in Fig. 9. Axial stress (σ_{xx}) and in-plane shear stress (τ_{xy}) contours at the concrete slab mid-height on a quarter of the twin-girder deck are shown in Fig. 10. It can be seen from these figures that the distributions of the in-plane stress σ_{xx} is not constant along the slab width as a consequence of the shear lag effects. In Figs. 9 and 10, the results obtained from the present finite element model are compared with the results of GBT [8]. It is worthy to note that the cross-section kinematic description in the GBT model is based on the superposition of so-called "cross-section deformation modes", whose amplitudes along the member axis are unknowns. GBT approach can effectively predicts the in-plane and out-of-plane cross-section deformations of thin-walled beams. It can be seen that the present finite element model results are in
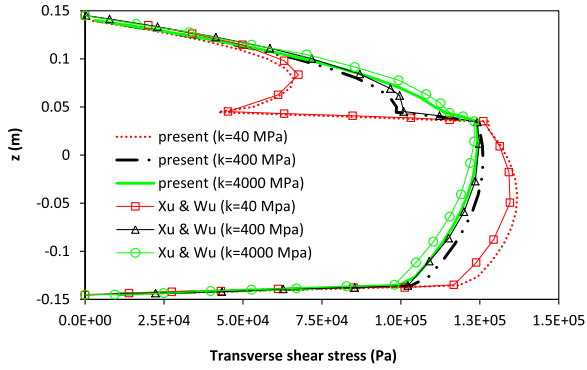
Table 2
Maximum slip, deflection, and shear stress of simply supported steel-concrete composite beam for different values of interfacial stiffness.

αL	Maximum deflection (mm)			Maximum slip (mm)			Maximum shear stress (MPa)		
	Present	TBT [10]	HBT [10]	present	TBT [10]	HBT [10]	present	TBT [10]	HBT [10]
0.1	21.10	22.50	23.03	2.3286	2.533	2.550	19.01	7.01	22.7
1	20.19	21.48	22.08	2.1330	2.318	2.334	18.85	6.98	22.5
5	13.61	14.20	14.65	0.7143	0.7705	0.7771	17.94	6.70	21.2
10	11.46	11.85	12.27	0.2404	0.2580	0.2611	17.81	6.59	20.7
20	10.72	11.04	11.45	0.0685	0.0732	0.0745	17.82	6.54	20.5
50	10.50	10.79	11.21	0.0119	0.0126	0.0130	17.87	6.50	20.3

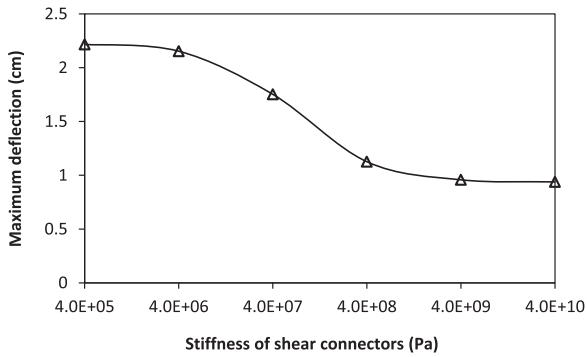**Fig. 6.** Through-the-thickness distributions of transverse shear stress at (0,0,z).

Fig. 7. Variations of the maximum deflection of composite beam with respect to the stiffness of the shear connectors.
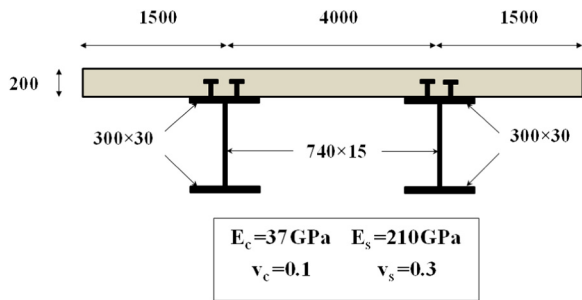

Fig. 8. Cross-section dimensions and material characteristic of the simply supported twin-girder composite deck (all dimensions in *mm*).
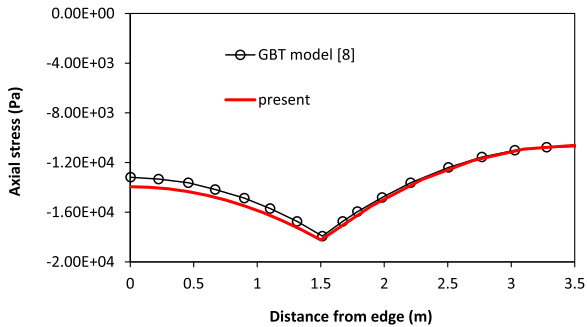

Fig. 9. Distributions of the mid-span axial stress σ_{xx} at the concrete slab mid-height.

good agreement with GBT results.

4.4. Two-span twin-girder composite deck

In this example, a realistic two-span twin-girder composite deck is analyzed using the proposed finite element model. The material properties, geometrical parameters, boundary and loading conditions of the composite deck are shown in Fig. 11. For analyzing this deck using the present finite element model, first the sensitivity of the numerical results with respect to the number of elements was carried out. Due to the symmetry, only a half of composite deck was modeled. It was found that the discretization of the deck into 40 equal sized beam elements yields results with enough accuracy. For comparison purposes, a 3D finite element analysis was also carried out using ABAQUS software. A mesh with 35,800 elements is shown in Fig. 12. Eight-node brick elements with linear elastic behavior were employed for modeling the concrete slab and steel joists while flexible shear connectors were modeled using appropriate contact (cohesive) elements with linear elastic traction-separation behavior. Traction-separation laws describe the interaction between two surfaces by defining a relative displacement at each contact point. The initial stiffness of the contact elements in normal and tangential directions are taken as $0.01 K_{nn} = K_{ss} = K_{tt} = k_w = 12 kN/mm^2$. For more details about contact elements and traction-separation behavior, interested readers can refer to [26]

Distributions of axial stress σ_{xx} along the width of the concrete slab at different sections of the composite deck are shown in Fig. 13. Longitudinal variations of the transverse deflection and axial stress in the bottom flange of the steel joists are depicted in Figs. 14 and 15, respectively. In these figures, the present results are compared with ABAQUS results. The comparison with 1D finite element results of Dezi et al. [5] is also made. Note that the kinematic description of the steel joist and concrete slab in Ref. [5] is based on the EBT. However, a known warping function is introduced in the kinematic of concrete slab for accounting the effects of shear lag. It can be observed from Figs. 14–15 that the results predicted by the present finite element model are in good agreement with ABAQUS results. Concerning Fig. 13.a, less accurate results are obtained for the regions near the free edge of concrete slab. This is due mainly to the presence of the transverse shear stress τ_{yz} in the concrete slab which is not considered in the present formulation. However, it is seen from Fig. 13.a that the results of the present finite element model in the prediction of the axial stress at the middle of composite deck is more accurate than in those obtained by Dezi et al. [5]. Since the kinematical formulations of Dezi et al. is based of EBT, it is not able to take into account the effects of transverse shear stress τ_{xz} in the concrete slab and steel joists. In contrast to model of Dezi et al., the present formulation uses a cosine function for representing the transverse shear stress in the concrete slab and steel joists. Other reason for existence of large difference between the present results and those of Dezi et al. is the use of different warping intensity function in formulation. In [5], the intensity of warping shape function is assumed to be constant on the slab thickness. In the present study, a warping intensity function with non-uniform distribution along the thickness of concrete slab is used for representing the shear lag phenomenon.

Through-the-thickness distributions of the transverse shear stress τ_{xz} and the axial displacement U are shown in Figs. 16–17. Distribution of the axial displacement at the end support of the composite deck with respect to y- coordinate is depicted in Fig. 18. Again, the agreement between the present and ABAQUS results is good. The simplifying assumptions that are used in the derivation of present finite element model (e.g. neglecting the effects of transverse shear stress τ_{yz} in the
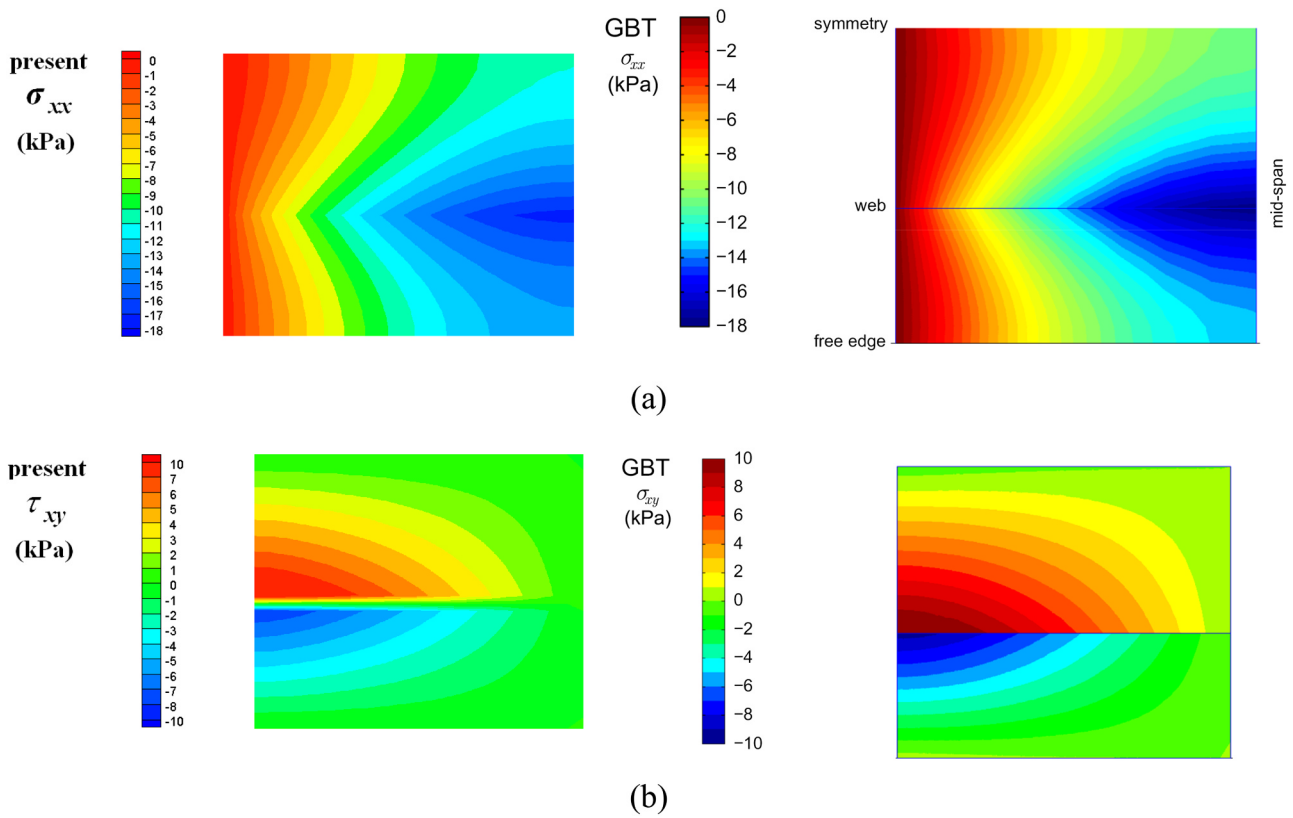
Fig. 10. Present and GBT [8] contours at the concrete slab mid-height: (a) axial stress σ_{xx}, (b) in-plane shear stress τ_{xy}.
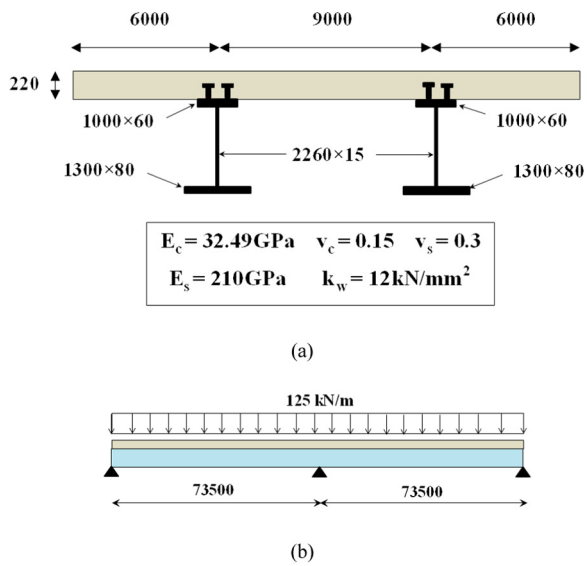

Fig. 11. Two-span twin-girder composite deck: (a) cross-section dimensions and material properties, (b) boundary and loading conditions (all dimensions in *mm*).
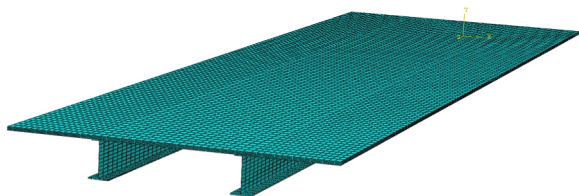

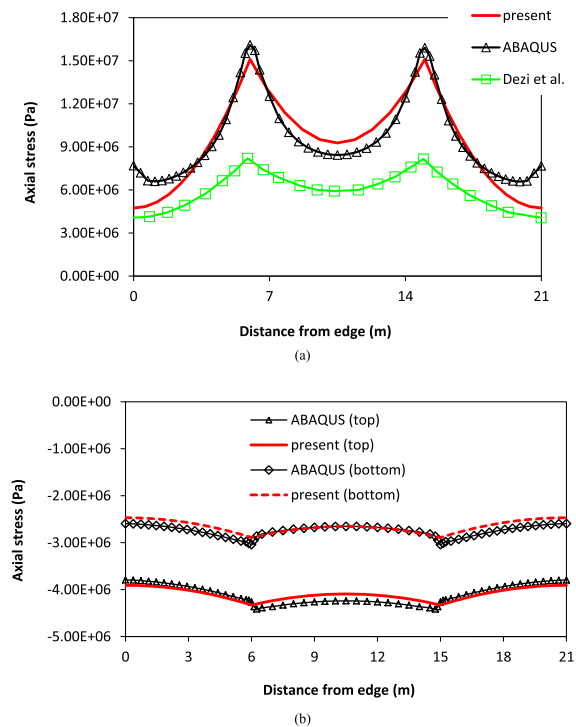**Fig. 12.** 3D finite element model of two-span twin-girder composite deck.

Fig. 13. Distribution of axial stress at different sections of the concrete slab: (a) at $(L/2, y + B, h_c/2)$, (b) at $(L/4, y, \pm h_c/2)$.

concrete slab and assuming a uniform distribution of the vertical displacement on the slab width) may be some reason for appearing discrepancy between the present and ABAQUS results. However, the converged mesh of ABAQUS has 144,000 dof. This value for the present
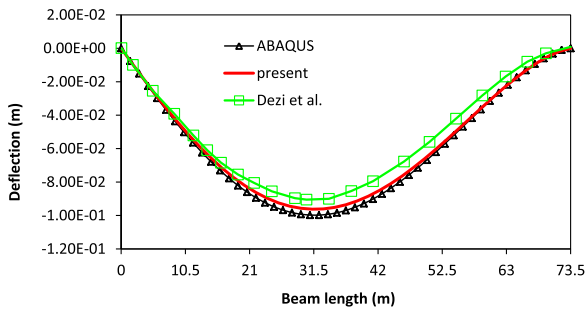
Fig. 14. Longitudinal variations of the transverse deflection of the two-span composite deck.
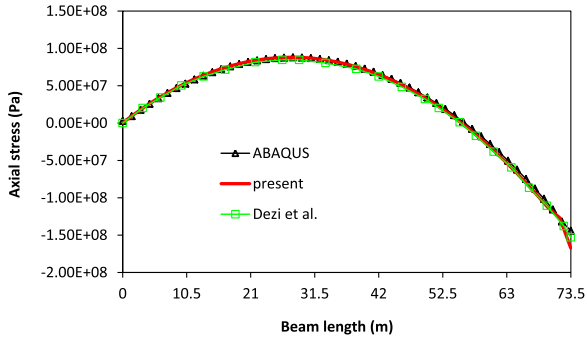

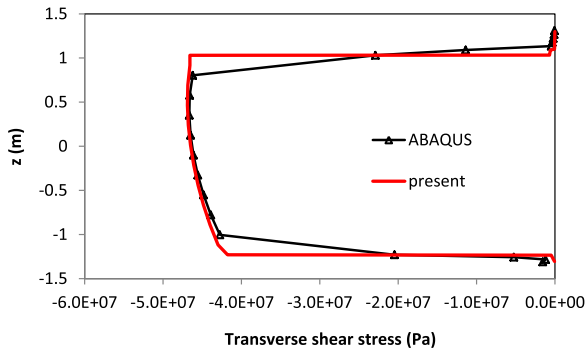**Fig. 15.** Longitudinal variations of the axial stress in the bottom flange of the steel joists.

Fig. 16. Distributions of the transverse shear stress $\sigma_{xz}(0, 0, z)$ along the height of the twin-girder composite deck.
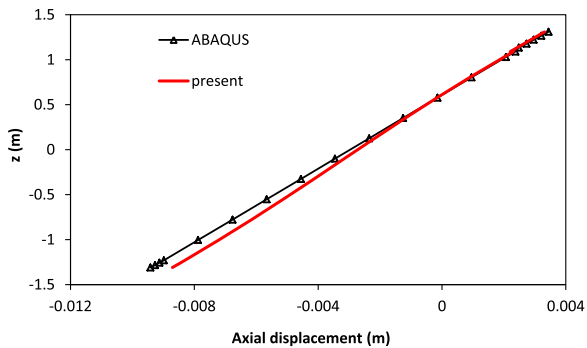

Fig. 17. Distributions of the axial displacement $U(0, 0, z)$ along the height of the twin-girder composite deck.

finite element model is 649. These results prove the efficiency of the present finite element model for the static analysis of twin-girder composite decks.

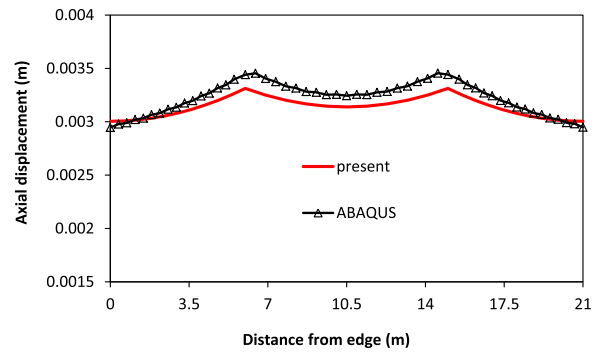Some useful data about the shear lag phenomenon can be found

Fig. 18. Distribution of the axial displacement at the top of the concrete slab - end support.
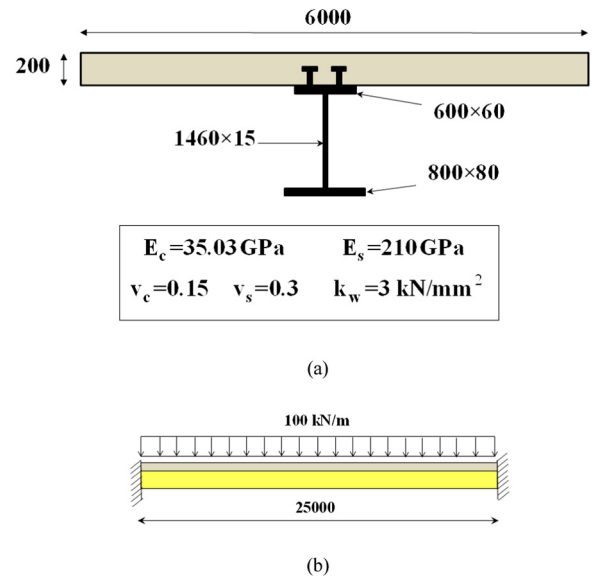

Fig. 19. Data of the clamped-clamped steel-concrete composite beam (all dimensions in *mm*).
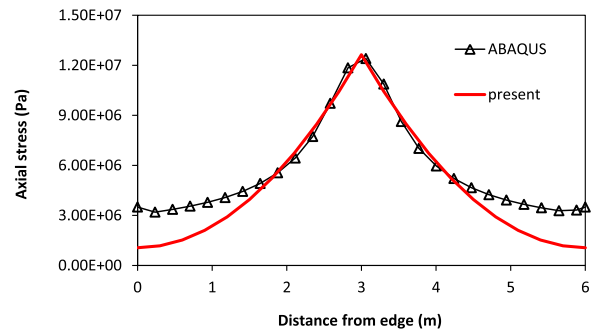

Fig. 20. Distribution of the axial stress at the top of concrete slab - end support $(L, y + B, h_c/2)$.

through comparing the axial stress distribution at the concrete slab of the present twin-girder composite beam (Fig. 9) with that obtained in the previous example (Fig. 13). The deck width-to-span ratio in the twin-girder composite beam of the present example ($2B/L = 0.286$) is much lower than the twin-girder composite one studied in the previous example ($2B/L = 0.875$). However, the axial stress concentration in the slab areas near the steel joists of the twin-girder composite beam of the present example is much higher than that one studied in the previous example. This shows that the deck width-to-span ratio is not only parameter which affects the intensity of the shear lag phenomenon in
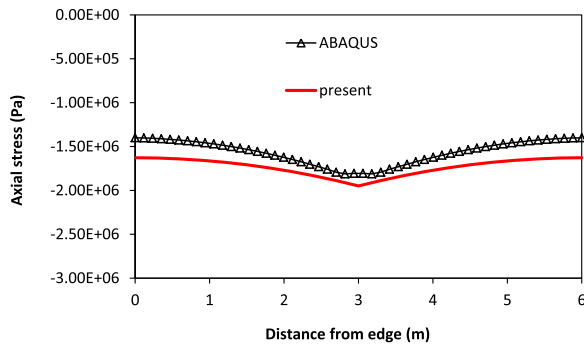
Fig. 21. Distribution of the axial stress at the top of concrete slab – mid span ($L/2$, $y + B$, $h_c/2$).

composite decks. It seems that beam's end conditions as well as the steel joist spacing (B_1/B) are other parameters which are effective on the warping of concrete slab cross-section.

4.5. Wide slab steel-concrete composite beam with fixed ends

As a final example, a wide slab steel-concrete composite beam with fixed ends is analyzed using the proposed finite element model. The geometrical parameters, elastic characteristics of the materials, loading and boundary conditions are shown in Fig. 19.

The considered steel-concrete beam was analyzed using 40 equal sized beam elements (649 dof). Distributions of the axial stress (σ_{xx}) along the wide of the concrete slab at two different sections of the beam are shown in Figs. 20–21. In these figures, the present results are compared with 3D finite element (ABAQUS) results. Similar to previous example, it is seen that the present results are in good agreement with ABAQUS results. However, the number of degrees of freedom in the ABAQUS model (35,400 dof) is much higher than in the present 1D finite element model.

It can be concluded from the above numerical results that the presented finite element model is able to predict the shear lag and interfacial slip phenomena in composite steel-concrete beams and twin-girder decks with enough accuracy. Indeed, the presented finite element model is simple and efficient for a low computational cost, compared to 3D finite element models available in commercial softwares.

5. Conclusion

Based on the sinus shear deformation beam theory, a 1D finite element model was developed for the static analysis of composite steel-concrete beams and twin-girder decks. The proposed finite element model incorporates shear lag phenomenon, slab-beam interfacial slips effects and the zero boundary conditions of the transverse shear stress on the top and bottom surfaces of the composite beam and deck without using shear correction factors. The shear lag phenomenon is captured through introducing appropriate warping function for the slab cross-section while the partial shear interaction between the slab and the steel beams is represented using the concept of spring layer model. In order to assess the accuracy of the present formulation, the results obtained from the present model were compared with other similar analytical and numerical models available in the literature. Further comparisons were also made with the results obtained from 3D finite element models. Comparison studies show that the present 1D beam finite element model gives quasi-3D solutions at a low computational

cost.

Future works are towards the extension of the proposed finite element model to the free vibration and materially nonlinear problems of the composite steel-concrete beams/decks.

References

[1] D.J. Oehlers, M.A. Bradford, Composite Steel and Concrete Structural Members: Fundamental Behavior, Pergamon Press, Oxford, 1995.
[2] X. Wang, F.G. Rammerstorfer, Determination of effective breadth and effective width of stiffened plates by finite strip analyses, Thin-Walled Struct. 26 (4) (1996) 261–286.
[3] F.F. Sun, O. Bursi, Displacement-based and two-field mixed variational formulation for composite beams with shear lag, J. Mech. Eng. 131 (2) (2005) 199–210.
[4] F.F. Sun, A beam element for steel-concrete composite beams with shear lag and area load, Proceedings of the Fourth International Conference on Advances in Steel Structures, Shanghai, China 13-15, 2005.
[5] L. Dezi, F. Gara, G. Leoni, A beam finite element for the shear lag analysis of steel–concrete composite decks, Proceedings of the Fourth International Conference on Advances in Steel Structures June, Shanghai, China 13–15, 2005.
[6] G. Fabrizio, L. Graziano, D. Luigino, A beam finite element including shear lag effect for the time-dependent analysis of steel-concrete composite decks, Eng. Struct. 31 (2009) 1888–1902.
[7] Q.Z. Luo, Y.M. Wu, Q.S. Li, J. Tang, G.D. Liu, A finite segment model for shear lag analysis, Eng. Struct. 26 (2004) 2113–2124.
[8] D. Henriques, R. Gonçalves, D. Camotim, A physically non-linear GBT-based finite element for steel and steel-concrete beams including shear lag effect, Thin-Walled Struct. 90 (2015) 202–215.
[9] Md Alhaz Uddin, A.H. Sheikh, D. Brown, T. Bennett, B. Uy, A higher order model for inelastic response of composite beams with interfacial slip using a dissipation based arc-length method, Eng. Struct. 139 (2017) 120–134.
[10] A. Chakrabarti, A.H. Sheikh, M. Griffith, D.J. Oehlers, Analysis of composite beams with partial shear interactions using a higher order beam theory, Eng. Struct. 36 (2012) 283–291.
[11] A. Zona, G. Ranzi, Finite element models for nonlinear analysis of steel–concrete composite beams with partial interaction in combined bending and shear, Finite Elem. Anal. Des. 47 (2011) 98–118.
[12] A.R. Da Silva, M. João Batista, Sousa Jr., A family of interface elements for the analysis of composite beams with interlayer slip, Finite Elem. Anal. Des. 45 (2009) 305–314.
[13] A. Dall'Asta, A. Zona, Slip locking in finite elements for composite beams with deformable shear connection, Finite Elem. Anal. Des. 40 (2004) 1907–1930.
[14] G. Ranzi, F. Gara, G. Leoni, A. Mark, Bradford, Analysis of composite beams with partial shear interaction using available modelling techniques: a comparative study, Comput. Struct. 84 (2006) 930–941.
[15] G. Taig, G. Ranzi, D. Dias-da-Costa, G. Piccardo, A. Luongo, A GBT model for the analysis of composite steel–concrete beams with partial shear, Interact. Struct. 4 (2015) 27–37.
[16] O. Polit, M. Touratier, High-order triangular sandwich plate finite element for linear and non-linear analyses, Comput. Methods Appl. Mech. Eng. 185 (2–4) (2000) 305–324.
[17] P. Vidal, O. Polit, A family of sinus finite elements for the analysis of rectangular laminated beams, Compos. Struct. 84 (1) (2008) 56–72.
[18] P. Vidal, O. Polit, A refined sine-based finite element with transverse normal deformation for the analysis of laminated beams under thermomechanical loads, J. Mech. Mater. Struct. 4 (6) (2009) 1127–1155.
[19] S.B. Beheshti-Aval, M. Lezgy-Nazargah, P. Vidal, O. Polit, A refined sinus finite element model for the analysis of piezoelectric-laminated beams, J. Intell. Mater. Syst. Struct. 22 (3) (2011) 203–219.
[20] M. Lezgy-Nazargah, P. Vidal, O. Polit, An efficient finite element model for static and dynamic analyses of functionally graded piezoelectric beams, Compos. Struct. 104 (2013) 71–84.
[21] M. Lezgy-Nazargah, S.M. Divandar, P. Vidal, O. Polit, Assessment of FGPM shunt damping for vibration reduction of laminated composite beams, J. Sound Vib. 389 (2017) 101–118.
[22] M. Lezgy-Nazargah, A generalized layered global-local beam theory for elasto-plastic analysis of thin-walled members, Thin-Walled Struct. 115 (2017) 48–57.
[23] M. Lezgy-Nazargah, L. Kafi, Analysis of composite steel-concrete beams using a refined high-order beam theory, Steel Compos. Struct. 18 (6) (2015) 1353–1368.
[24] M. Lezgy-Nazargah, An isogeometric approach for the analysis of composite steel–concrete beams, Thin-Walled Struct. 84 (2014) 406–415.
[25] R.Q. Xu, Y.F. Wu, Two-dimensional analytical solutions of simply supported composite beams with interlayer slips, Int. J. Solids Struct. 44 (1) (2007) 165–175.
[26] Hibbitt, Karlsson, and Sorensen, Inc., ABAQUS Theory manual, User manual and Example Manual, Version 6.7. Providence, RI, 2000.